Fuel 320 (2022) 123900

Contents lists available at ScienceDirect

Fuel

journal homepage: www.elsevier.com/locate/fuel

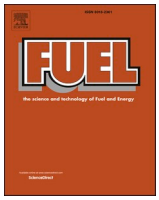

Full Length Article

Efficient production of hydrogen from a valuable CO_2-derived molecule: Formic acid dehydrogenation boosted by biomass waste-derived catalysts

Jessica Chaparro-Garnica [a,1], Miriam Navlani-García [a,1,*], David Salinas-Torres [b,c], Ángel Berenguer-Murcia [a,*], Emilia Morallón [b], Diego Cazorla-Amorós [a]

[a] Departamento de Química Inorgánica e Instituto de Materiales, Universidad de Alicante, Apartado 99, Alicante E-03080, Spain
[b] Departamento de Química Física e Instituto de Materiales, Universidad de Alicante, Apartado 99, Alicante E-03080, Spain
[c] Departamento de Ingeniería Química y Ambiental, Universidad Politécnica de Cartagena, Cartagena, E-30202, Spain

ARTICLE INFO

Keywords:
CO_2 valorization
Formic acid
Hydrogen
Carbon materials
Metal nanoparticles
Biomass waste

ABSTRACT

Formic acid has been postulated as one of the most promising liquid organic hydrogen carriers. Numerous studies dealing with the development of efficient catalysts able to boost the dehydrogenation of formic acid can be found in recent literature. However, most of them lack in stability, so that finding stable catalysts is highly desirable yet challenging. In the present study, we developed Pd-based biomass-derived carbon-supported catalysts by following a simple protocol. The effect of the modification of both the metal phase and support has been assessed by incorporating Ag in the form of bimetallic nanoparticles and nitrogen functional groups, respectively. The effect of the method followed for the preparation of the catalysts was also checked. It has been found that the resulting PdAg-based catalysts supported on N-doped biomass-derived carbon materials showed suitable activity and excellent stability under reaction conditions. The present study highlights the potential of modulating the features of the catalysts, not only in terms of the composition of the metal phase and incorporation of heteroatoms in the support, but also in terms of the synthetic protocol used.

1. Introduction

Carbon dioxide (CO_2) is recognized as one of the main greenhouse gases (GHGs), which is not due to its global warming potential (GWP) that is much lower than that of other gases (i.e. GWP of 1, 28–36, and 265–298, for CO_2, CH_4, and N_2O, respectively) [1], but because of the much larger contribution of CO_2 to the total emissions of GHGs (i.e. CO_2 accounts for ~ 76% of total GHGs emissions, while CH_4, and N_2O account for 16 and 6 %, respectively) [2], and the larger net energy absorption of CO_2 due to its longer permanency in the atmosphere compared to other GHGs [3].

CO_2 is part of the carbon cycle on Earth, so it is naturally present in the atmosphere. However, anthropogenic activities are dramatically increasing its concentration, thus altering said cycle. Most of the CO_2 emission derived from anthropogenic activities comes from the combustion of fossil fuels (i.e. coal, oil, and natural gas) for transportation, energy, and industry-related applications [4]. Hence, considering the ever-increasing global energy demands, limiting the concentration of CO_2 in the atmosphere seems inconceivable unless a radical change is produced in the global lifestyle and current energy system. Among the solutions contemplated for the control of CO_2 emissions, its conversion into fuels and chemicals is an auspicious alternative to minimize the impact of CO_2 in the greenhouse effect while obtaining valuable molecules. Catalytic conversion of CO_2 has become one of the central challenges addressed by the research community [5–7] Among the possible pathways, the hydrogenation of CO_2 into formic acid (HCOOH, FA) by means of chemical, photochemical, and electrochemical routes is receiving increasing attention over the last years [8], which is due to the extraordinary properties of formic acid and its potential role as a platform for chemical hydrogen storage.

FA is nowadays recognized as one of the most promising hydrogen carrier molecules, as well as a molecule that, coupled to CO_2, would be involved in an ideal carbon–neutral cycle *via* hydrogenation and dehydrogenation reactions [9]. The latter path (i.e. dehydrogenation of FA) has recently become a central topic of research. Many catalysts formulations have already been reported to afford relatively high FA

* Corresponding authors at: Departamento de Química Inorgánica e Instituto Universitario de Materiales, University of Alicante, P.O. Box 99, San Vicente del Raspeig, E-03080 Alicante, Spain.
E-mail addresses: miriam.navlani@ua.es (M. Navlani-García), a.berenguer@ua.es (Á. Berenguer-Murcia).
[1] Authors contributed equally to this work.

https://doi.org/10.1016/j.fuel.2022.123900
Received 27 December 2021; Received in revised form 7 March 2022; Accepted 15 March 2022
Available online 19 March 2022

conversion and selectivity towards the dehydrogenation of FA into H_2 and CO_2 (i.e. suppressing the undesired dehydration side reaction; $HCOOH \leftrightarrow H_2O + CO$). Catalysts based on Pd nanoparticles are the preferred option, since they have shown good results when supported on materials of diverse nature (i.e. zeolites [10], oxides [11,12]; Metal-Organic Frameworks (MOFs) [13,14], resins [15–17], carbon materials [18–21], etc.). In an effort to overcome the limitation of most of the catalysts, that is, their poor stability under reaction conditions, several approaches that involve the modification of the support and/or the control of the metal active phases have already been addressed. Among the modification of the supports, the incorporation of nitrogen functional groups has given excellent results [22–24], while the deployment of bimetallic nanoparticles has been the most fruitfully investigated option towards the optimization of the properties of the metal active phase [15,19,25,26]. In this regard, PdAg-based nanoparticles have attracted significant attention in this reaction because the combination of Pd with Ag results in electron-rich Pd species produced by the difference in electronegativity of both elements. Furthermore, such electron-rich Pd species favour some steps of the formic acid dehydrogenation reaction [15,25]. Despite the great efforts devoted, most of the catalysts used for the dehydrogenation of FA have shown poor long-term stability.

We recently developed efficient catalysts based on Pd nanoparticles supported on nitrogen-doped (N-doped) biomass waste-derived carbon materials [27,28]. It was observed that the designed monometallic Pd catalysts showed great stability under reaction conditions. Herein, we further explore the suitability of catalysts based on carbon materials derived from biomass waste by developing bimetallic PdAg-based catalysts. In order to get an insight into the effect of the properties of both support and metal active phase, both N-free and N-doped carbon-supported catalysts were prepared, and the metal nanoparticles were loaded by both pre-reduction with a strong reducing agent (i.e. $NaBH_4$) and *in-situ* reduction during the dehydrogenation of FA. It was observed that, upon selection of the experimental conditions used in the synthesis of the samples, catalysts with suitable activity and excellent stability were obtained. The modulation of the properties of the catalysts by both introducing Ag in the metal phase, as well as the incorporation of heteroatoms in the support, in the form of N-functional groups, showed great potential in attaining very promising catalysts for the production of hydrogen from the dehydrogenation of FA in liquid phase.

2. Experimental

2.1. Preparation of biomass-derived activated carbon and N-doped activated carbon

The biomass-derived activated carbon was obtained from almond shells (AS) by H_3PO_4-assisted HydroThermal Carbonization (HTC) following the procedure described in previous studies [27–29]. The synthesis was performed by mixing 1 g ± 0.001 g of AS with 8 g ± 0.001 g of an aqueous solution of 25 wt % in H_3PO_4 in a 50 mL Teflon-lined stainless-steel autoclave (weight ratio of H_3PO_4/AS equal to 2) and futher heat treatment up to 450 °C. The as-synthesised activated carbon was denoted as AS. The N-doped activated carbon was subsequently prepared through an organic reaction under mild conditions as described elsewhere [29]. The resulting N-doped carbon was denoted as N-AS.

2.2. Preparation of Pd and PdAg catalysts

Pd and PdAg catalysts were prepared on both AS and N-AS supports, by using $Pd(OAc)_2$ and $AgNO_3$ as metal precursors. To check the effect of the preparation method, two sets of samples were synthesized for both mono- and bimetallic catalysts. In the first set of catalysts, $NaBH_4$ was used as a reducing agent after the impregnation of the support with the metal precursors. The samples were denoted as Pd/AS, Pd/N-AS, PdAg/AS, PdAg/N-AS, for monometallic and bimetallic catalysts, respectively, and according to the nomenclature given to the supports. In the case of the second set of catalysts, the reduction step with $NaBH_4$ was skipped and the metal phases were *in-situ* reduced under reaction conditions during the FA dehydrogenation reaction. The as-synthesized catalysts were denoted as Pd/AS(n.r.), Pd/N-AS(n.r.), PdAg/AS(n.r.), PdAg/N-AS (n.r.), for monometallic and bimetallic catalysts, respectively, and according to the nomenclature given to the supports, and with "n.r" standing for "non-reduced". All catalysts had a nominal Pd loading of 1 wt % and, in the case of bimetallic catalysts, a Pd/Ag molar ratio of 1/0.5 was selected. Thus, a total of 8 catalysts were prepared to explore the effect of (1) composition of the metal active phase as either monometallic Pd or bimetallic PdAg nanoparticles, (2) nitrogen incorporation in the support in both monometallic and bimetallic PdAg catalysts, and (3) effect of the synthesis of the catalysts by using pre-reduced and *in-situ* reduced catalysts.

2.3. Characterization of the materials

The porous texture of the supports was analyzed by physical adsorption–desorption of N_2 at −196 °C with an automatic adsorption system (Micromeritics ASAP 2020 analyzer). Before analysis, samples were degassed at 200 °C for 6 h. The apparent surface area and total micropore volume (V_{DR} N_2) were calculated applying the Brunauer-Emmett-Teller (BET) method and the Dubinin–Radushkevich (DR) equation to the N_2 adsorption isotherm at −196 °C, respectively. Mesopore volume was determined by calculating the difference between the volume of N_2 adsorbed at a relative pressure of 0.95 and the micropore volume [30]. Pore size distributions were obtained from the 2D-NLDFT heterogeneous surface model using the SAIEUS software (available online at http://www.nldft.com/) [31]. Transmission Electron Microscopy was used to check the morphology of the catalysts and a JEOL (JEM-2010) transmission electron microscope operating at 200 kV with a spatial resolution of 0.24 nm was used. Average nanoparticle size and size distribution were calculated after measuring ~ 100 individual nanoparticles. The dispersion of Pd nanoparticles (D), defined as the number of Pd atoms on the surface of the sample divided by the total number of Pd atoms, was estimated by assuming spherical nanoparticle geometry [32]. Pd and Ag content was determined by Inductively Coupled Plasma-Optical Emission Spectroscopy (ICP-OES) with a Perkin-Elmer Optima 4300 system. ICP-OES analysis was repeated three times for proper quantification of the metal content. X-ray photoelectron spectroscopy (XPS) analysis was performed in a VG-Microtech Multilab 3000 spectrometer equipped with a semispherical electron analyzer and a Mg Kα ($h\nu = 1253.6$ eV) 300 W X-ray source. Binding energies were referred to the C 1s line at 284.6 eV in all cases. N 1s and Pd 3d spectra were analysed.

2.4. Catalytic tests

The prepared catalysts were assessed in the dehydrogenation of FA in the liquid phase at 75 °C. The reaction was monitored for 30 min by registering the gas evolved at fixed times. The catalytic tests were carried out using 0.150 g ± 0.001 g of catalyst and an aqueous solution of formic acid and sodium formate with a molar ratio of 9 to 1 with a final concentration of 1 M. The stability of the catalysts was evaluated by performing six consecutive reaction runs. For that, the spent catalyst was collected by filtration and a fresh solution of formic acid-sodium formate was used for the next cycle. The volume of gas generated ($H_2 + CO_2$) was normalized per gram of catalyst to correct the effect of the loss of sample during their recovery.

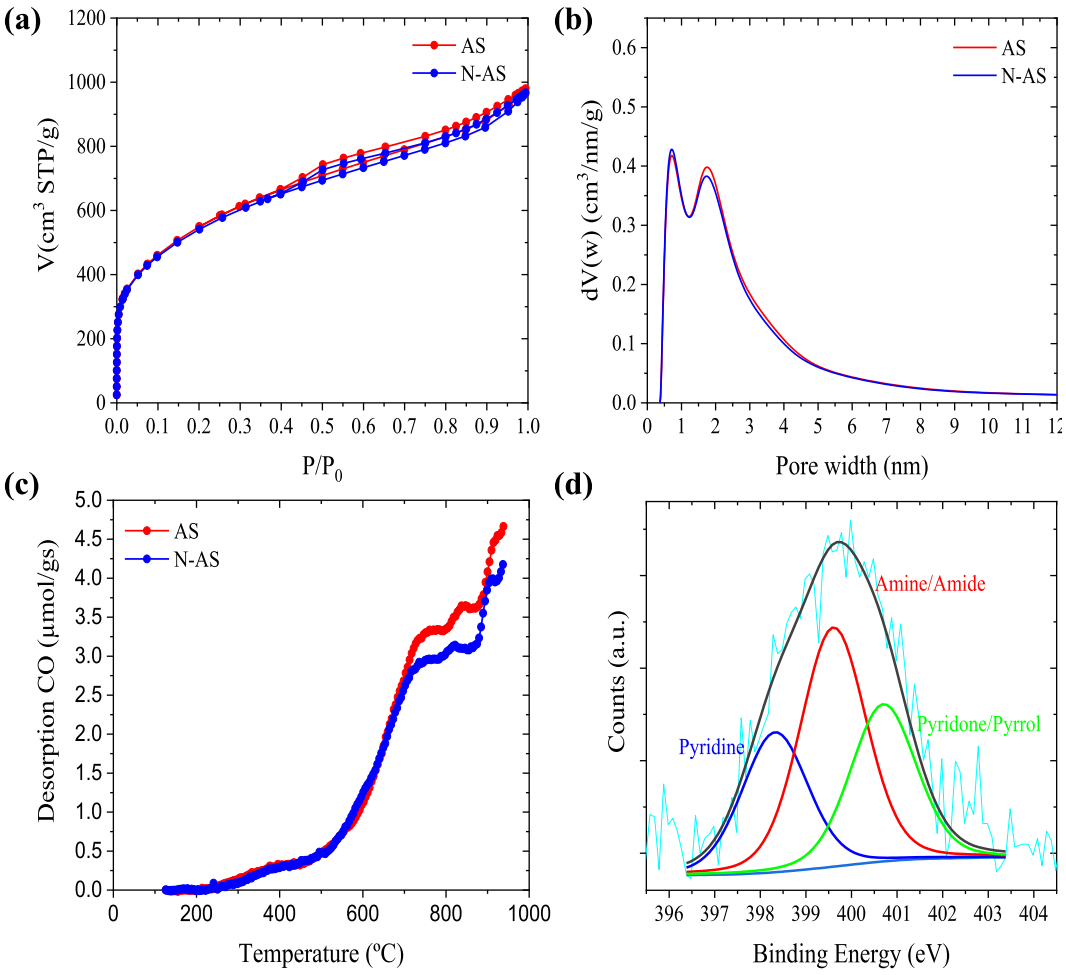

Fig. 1. Characterization of AS and N-AS supports: (a) N_2 adsorption–desorption isotherms at −196 °C of AS and N-AS supports; (b) Pore size distribution of AS and N-AS; (c) TPD profile; (d) N 1s XPS spectra of N-AS.

3. Results

Fig. 1 includes the results of the characterization of AS and N-AS supports. Fig. 1(a) shows the adsorption–desorption isotherms of N_2 at −196 °C as well as the pore size distribution. Both supports showed a Type I isotherm, characteristic of microporous solids. In addition, a hysteresis loop, associated with the presence of mesopores, could also be seen, indicating that these samples presented a combination of Type I and IV isotherms. Pore size distributions plotted in Fig. 1(b) (PSDs) profiles showed a bimodal distribution with a first peak at around 1 nm and a region of pore sizes higher than 2 nm, which derived from the presence of mesopores. The apparent surface area (S_{BET}) was calculated to be of 2010 ± 13 and 1980 ± 13 m^2/g, and the micropore volume (V_{DR} N_2) was 0.76 ± 0.03 and 0.75 ± 0.03 cm^3/g, for AS and N-AS samples, respectively, which suggested that the introduction of nitrogen functional groups did not change considerably the porous texture of the AS-derived activated carbon. The TPD profiles recorded for the AS and N-AS supports are depicted in Fig. 1(c). The quantification of the oxygen groups through TPD analysis for AS and N-AS was 3868 ± 118 $\mu molg^{-1}$ and 3720 ± 118 $\mu molg^{-1}$, respectively. This indicates that N functionalization is produced by the reaction with oxygen functional groups, mainly with CO-type groups which are the most abundant in both supports. In Fig. 1(c), it can be seen that AS CO desorption occurs from 300 °C. AS is rich in phenol groups, which evolve as CO between 600 °C and 700 °C, and in carbonyl groups that are desorbed at higher temperatures. After functionalization (N-AS), a decrease in the evolution of CO was observed at high temperatures, which indicates that phenol and carbonyl groups are consumed during the functionalization reaction, confirming that the generation of nitrogen groups are produced by substitution reactions with these oxygen groups [29].

N 1s XPS spectrum of N-AS is plotted in Fig. 1(d). The nitrogen surface content was determined to be ~ 1.4 ± 0.1 at.%. As it can be seen in Fig. 1(d), the N 1s XPS spectrum displayed three contributions, which can be attributed to the presence of pyridone/pyrrole, amine/amide, and pyridine groups, with a relative proportion of 19, 47, and 34 %, respectively.

ICP analysis (results shown in Table 1) confirmed that both Pd and Ag were successfully loaded in the catalysts, and that the Pd and Ag contents were similar in all cases (from 0.72 ± 0.01 to 0.83 ± 0.01 wt % for Pd, and from 0.32 ± 0.01 to 0.37 ± 0.01 wt % for Ag). The metal loading was close to the desired Pd/Ag molar ratio of 1/0.5 in all samples.

Table 1
Pd and Ag loading determined by ICP analysis.

Catalyst	Pd loading (wt %)	Ag loading (wt %)
Pd/AS	0.72 ± 0.01	–
Pd/AS (n.r.)	0.81 ± 0.01	–
Pd/N-AS	0.80 ± 0.01	–
Pd/N-AS (n.r.)	0.81 ± 0.01	–
PdAg/AS	0.78 ± 0.02	0.32 ± 0.01
PdAg/AS (n.r.)	0.83 ± 0.01	0.37 ± 0.01
PdAg/N-AS	0.79 ± 0.01	0.36 ± 0.01
PdAg/N-AS (n.r.)	0.80 ± 0.01	0.33 ± 0.01

The catalytic behavior of the as-prepared monometallic and bimetallic samples, with both pre-reduced and *in-situ* reduced (denoted as "n.r.", standing for "non-reduced") metal nanoparticles was assessed in the dehydrogenation of FA in the liquid phase by registering the gas evolution profiles (H_2 + CO_2) during 30 min. The results achieved for all samples in the first reaction cycle are plotted in Fig. 2. While the catalytic activity may be more accurately described if expressed per active site, our work shows the catalytic activity per gram of catalyst. This was done because Ag, while not active in the formic acid dehydrogenation reaction, does adsorb CO, which would lead to an inaccurate estimation of the surface active sites in the case of bimetallic nanoparticles, and hence a potentially misleading value of the catalytic activity expressed per active site.

The achieved profiles evidenced several effects. From the data included in Fig. 2(a), it can be observed that none of the catalysts with reduced nanoparticles exhibited an induction time and the gas evolved smoothly from the beginning of the registered reaction time. Monometallic N-free catalyst (Pd/AS) produced 234 mL_{gas}/g_{cat} after 30 min of reaction, while a much larger volume of gas was generated upon the incorporation of either N or Ag in the catalysts (607 and 745 mL_{gas}/g_{cat}, for Pd/N-AS and PdAg/AS, respectively), which demonstrated the great potential of both modifications of Pd-based catalysts in attaining excellent catalytic performance towards the dehydrogenation of FA. It should be noted that such an enhancement of the catalytic activity is further pronounced after the incorporation of both N and Ag in PdAg/N-AS (988 mL_{gas}/g_{cat}), indicating the synergistic effect of N and Ag in the catalyst. The beneficial effect of the incorporation of nitrogen functional groups had already been observed in our previous studies on biomass waste-derived carbon-supported Pd catalysts using a hemp residue as the starting material [27,28], as well as in other works in which different carbon materials were used as supports [21–23,33]. As previously claimed, nitrogen functional groups can modify the basicity of the catalysts thus favouring the interaction of FA molecules with the surface of the sample. Furthermore, they can be actively involved in the deprotonation of FA [27]. On the other hand, the presence of Ag in the form of bimetallic PdAg catalysts has also been reported to result in improved performance compared to the monometallic Pd counterparts [14,15,25]. For instance, it was previously observed that the presence of Ag in the bimetallic PdAg nanoparticles could modify both the electronic properties and size of the resulting nanoparticles [19]. Such effects will be discussed below. An interesting effect was seen when comparing the catalysts with pre-reduced nanoparticles (Fig. 2(a)) with those with non-pre-reduced nanoparticles (Fig. 2(b)). As observed in Fig. 2(b), an induction time was needed in this case, during which hydrogen evolved from the dehydrogenation of FA may be partially consumed in the reduction of the metal species at the beginning of the reaction. Comparing Pd/AS (n.r.) with Pd/N-AS (n.r.), it can be clearly seen that such a reduction is much more hampered (i.e. longer induction time) in the N-containing catalyst, which is in good agreement with previous results achieved for other Pd-based catalysts [27] and with the role of nitrogen atoms in stabilizing cationic Pd species [22]. After such an induction time, Pd/N-AS (n.r.) shows a sharp increase in the generation of gas, reaching a total volume of 693 mL_{gas}/g_{cat} after 30 min of reaction, which is much larger than that of the N-free non-reduced counterpart catalysts (Pd/AS (n.r.), 399 mL_{gas}/g_{cat}) and the equivalent catalysts with pre-reduced nanoparticles (Pd/N-AS, 607 mL_{gas}/g_{cat}). Those results again confirm the beneficial role of nitrogen and suggest the importance of the protocol used in the reduction of the metal species. According to that observation, *in-situ* reduced monometallic species display better performance than those pre-reduced nanoparticles, which were attained after using a strong reducing agent (i.e. $NaBH_4$). That may be due to the presence of more active (i.e. "clean") Pd metal species resulting when the reduction is carried out with the H_2 produced in the reaction rather than when an additional reducing agent is used. Interestingly, PdAg-catalysts showed a different tendency. As evidenced by the results plotted in Fig. 2(a) and (b), the pre-reduction of PdAg catalysts is mandatory to achieve very active bimetallic species under the experimental conditions used in this study, while the activity of the samples is significantly hindered when non-pre-reduced PdAg nanoparticles are present in the samples. According to these results, it may appear that the *in-situ* reduction of PdAg species with the H_2 evolved from the dehydrogenation of FA is not suitable to afford efficient catalysts for this reaction, which might be due to the possible formation of non-interacting and/or segregated Pd and Ag species and/or particles with suboptimal size or electronic properties for the studied reaction. However, since Ag is not active for the dehydrogenation of FA, the poor activity of PdAg/AS (n.r.) and PdAg/N-AS (n.r.) could be also attributed to the formation of Ag-rich surface nanoparticles, and thus inactive-rich species in the surface of the nanoparticles. The Pd/Ag ratio on the surface of the samples was determined from the XPS results. It was estimated that the surface Pd/Ag ratio was 1.30, 0.45, 1.36, and 1.06, for PdAg/AS, PdAg/AS(n.r.), PdAg/N-AS, PdAg/N-AS(n.r.), respectively. This indicates that the reduced samples showed more surface Pd species compared to the non-reduced counterpart, which is in good agreement with their better activity.

In order to further evaluate the performance of the developed catalysts, six consecutive reaction cycles were followed with all of the assessed samples. The results of the reusability tests for the two sets of

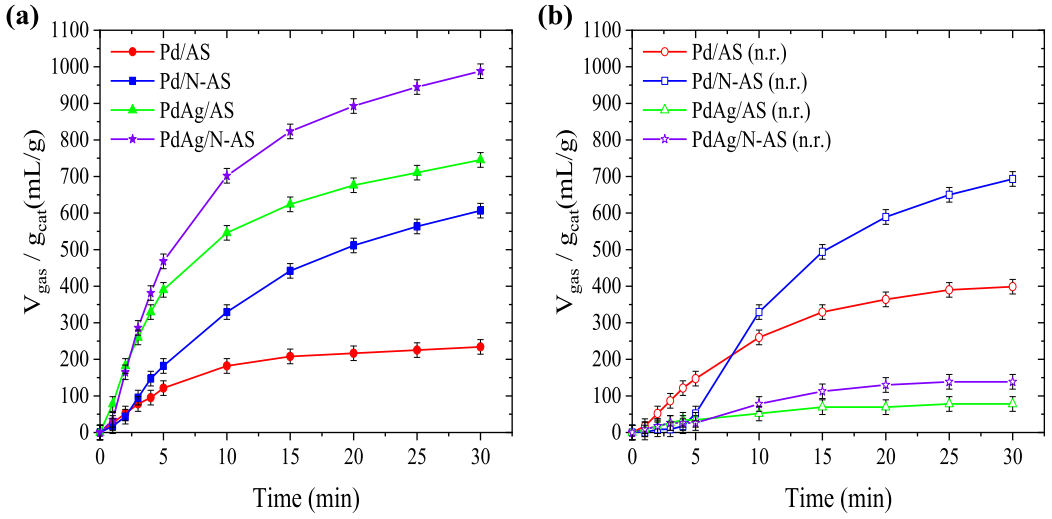

Fig. 2. Gas evolution profiles (H_2 + CO_2) achieved for: (a) Catalysts with pre-reduced nanoparticles; (b) Catalysts with *in-situ* reduced nanoparticles.

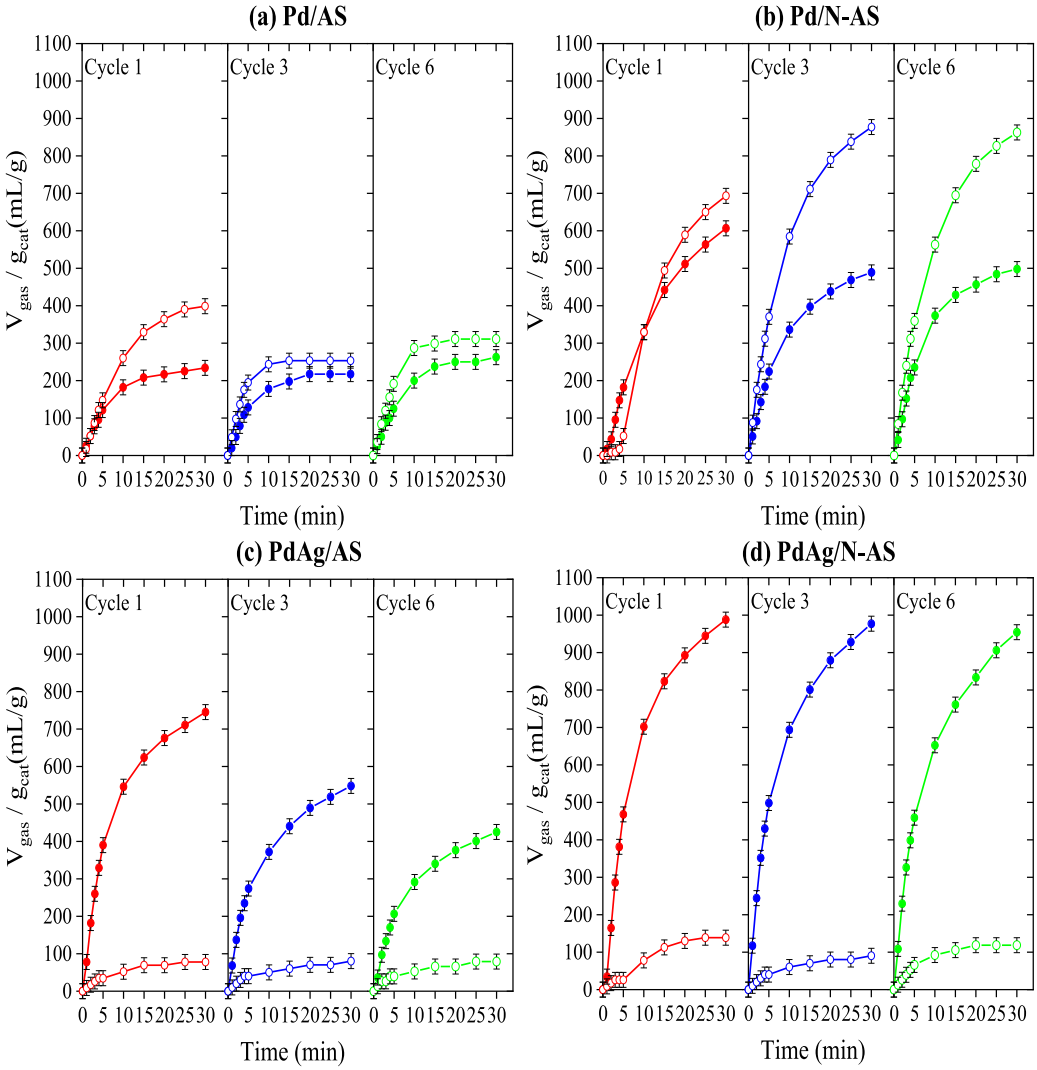

Fig. 3. Gas evolution profiles (H_2 + CO_2) for: (a) Pd/AS; (b) Pd/N-AS; (c) PdAg/AS; and PdAg/N-AS. Solid symbols (■) are used for catalysts with pre-reduced nanoparticles and hollow symbols (□) for the catalysts with non-pre-reduced nanoparticles (n.r.).

samples are depicted in Fig. 3. The obtained profiles help to evidence that, in the case of monometallic Pd catalysts, non-pre-reduced catalysts displayed better activity than those with pre-reduced nanoparticles, for both N-free and N-containing catalysts (Fig. 3(a) and (b)). However, as previously discussed, such a tendency was not seen for bimetallic PdAg catalysts, regardless of the presence of nitrogen in the samples (Fig. 3(c) and (d)). As revealed by the gas evolution profiles achieved, PdAg/N-AS catalyst is the most active among investigated, since it may fully benefit from both the effect of the nitrogen surface groups and the incorporation of Ag in the form of PdAg nanoparticles. That sample has an initial TOF value of 1577 h^{-1}, which is much higher than that calculated for the other catalysts with pre-reduced nanoparticles (i.e. 1379, 602, and 432 h^{-1} for PdAg/AS, Pd/N-AS, and Pd/AS, respectively) and those with non-pre-reduced nanoparticles. Also, the initial TOF achieved by PdAg/N-AS is higher than the values reported for other PdAg-based catalysts found in other studies (i.e. $Ag_{0.1}Pd_{0.9}$ nanoparticles assembled on reduced graphene oxide ($Ag_{0.1}$-$Pd_{0.90}$/rGO), TOF of 105 h^{-1} [34]; bimetallic AgPd alloy nanoparticles supported on carbon nitride (Ag_1Pd_2/CN), TOF of 621 h^{-1} [35]; PdAg alloy and MnO_x nanoparticles supported on aminopropyl-functionalized silica (PdAg-MnO_x/N-SiO_2), TOF of 700 h^{-1} [36]; Pd_1Ag_2 nanoparticles supported on commercial activated carbon (Pd_1Ag_2/C(1)), TOF of 855 h^{-1} [19]; Ag-Pd alloy supported on an amine-functionalized UiO-66 (AgPd@NH_2-UiO-66), TOF of 893 h^{-1} [37]; bimetallic nanoparticle functionalized zeolitic imidazolate framework (ZIF) derived N-decorated nanoporous carbon (AgPd@NPC), TOF of 936 h^{-1} [38]; PdAg alloy nanoparticles anchored on NH_2-functionalized 2D/2D TiO_2 nanosheet/rGO composite (Pd_8Ag_1/NH_2-TNS-rGO) 1090 h^{-1} [39]; etc.).

Not only does the catalytic activity of PdAg/N-AS deserve mention, but also its great stability (Fig. 3 (d)). It should be mentioned that all the developed catalysts showed good stability and they preserved their activity after six consecutive reaction cycles, which is a remarkable result. In our previous study [27], we found that the developed biomass-derived carbon-supported Pd catalysts presented outstanding stability and that such great stability under reaction conditions was further enhanced upon the incorporation of nitrogen functional groups in the catalysts. Herein, we further demonstrated that the followed approach can be extended to bimetallic PdAg catalysts. As seen in Fig. 3 (c) and (d) for PdAg catalysts with pre-reduced nanoparticles, N-free catalysts (PdAg/AS) displayed a catalytic activity decay of ~ 43 % in terms of the total volume of gas generated after 30 min of reaction (745 mL_{gas}/g_{cat} in the 1st reaction run and 425 mL_{gas}/g_{cat} in the 6th reaction run), while the activity loss shown by the N-containing counterpart (PdAg/N-AS) is almost negligible (~3 %; 988 mL_{gas}/g_{cat} in the 1st reaction run and 954 mL_{gas}/g_{cat} in the 6th reaction run). It should be noticed that the great stability shown by the studied bimetallic catalysts is a lacking aspect in

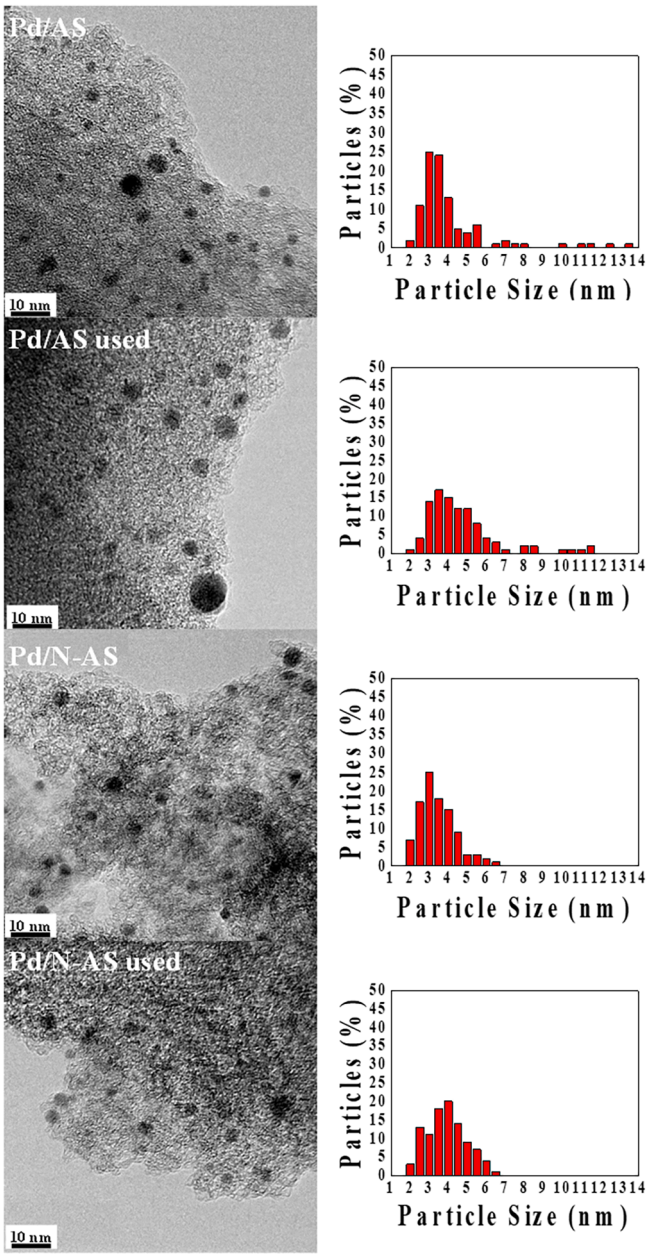

Fig. 4. TEM micrographs and pertinent histograms with the nanoparticle size distribution registered for fresh and used Pd/AS and Pd/N-AS catalysts.

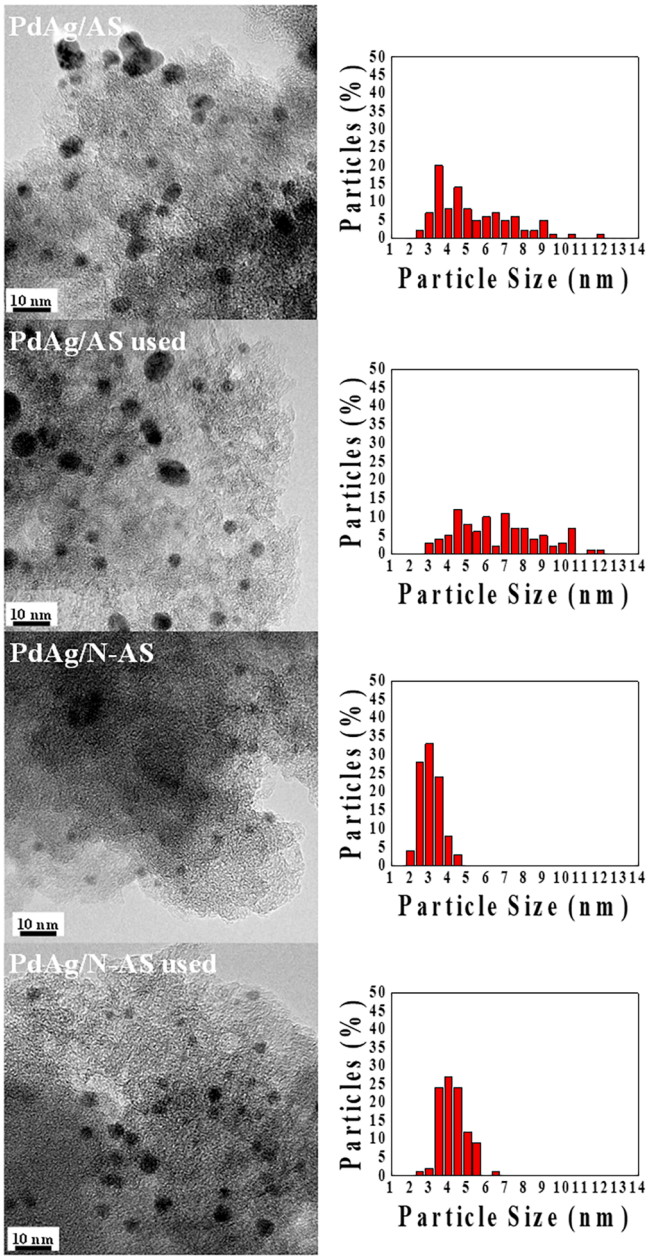

Fig. 5. TEM micrographs and pertinent histograms with the nanoparticle size distribution registered for fresh and used PdAg/AS, and PdAg/N-AS catalysts.

most of the systems studied elsewhere for the present application and it is an aspect that is frequently overlooked for PdAg by performing fewer consecutive reaction runs (i.e. 2 cycles were analysed for $Ag_{0.25}Pd/WO_3$ [40]; 3 cycles were evaluated for $Ag_{74}Pd_{26}$/graphene [41] and $Ag_{0.1}Pd_{0.9}$/N-ompg-C_3N_4 [42]; 4 cycles were assessed for Ag@Pd/N-GCNT [43]; 5 cycles for PdAg-CeO_2 [44], Ag_1Pd_9-$(MnOx)_{1.5}$/A-CS [45], AgPd@ZIF-8 [46], and Ag_1Pd_9/SBA-15-Amine [47]) or even obviated [19,34,48–51].

In order to get further insight into the properties of the catalysts that govern the catalytic performance, fresh and spent catalysts were characterized. Fig. 4 and Fig. 5 include the TEM micrographs registered for fresh and used catalysts with pre-reduced nanoparticles Pd and PdAg-based, respectively. The average nanoparticle size (d_{TEM} (nm)) and the dispersion (D (%) of these samples together with that determined for the spent catalysts which were *in-situ* reduced with the hydrogen evolved from the reaction is listed in Table 2.

As can be seen in the TEM micrographs (Fig. 4 and Fig. 5) and in the data included in Table 2, all the fresh samples with pre-reduced nanoparticles display small and well-dispersed nanoparticles with an average particle size ranging from 2.8 ± 0.5 to 5.0 ± 2.0 nm. In the case of the catalysts with monometallic nanoparticles (Pd/AS and Pd/N-AS), the N-containing catalyst presented smaller nanoparticle sizes than the N-free counterpart (3.2 ± 0.9 and 3.8 ± 2.1 nm for Pd/N-AS and Pd/AS). Such an effect of the N-functional groups in attaining small nanoparticles is more pronounced by comparing the catalysts with bimetallic PdAg nanoparticles (2.8 ± 0.5 and 5.0 ± 2.0 nm for PdAg/N-AS and PdAg/AS, respectively). Also, the presence of nitrogen in the support help attain a narrower particle size distribution, which can be clearly seen in the histograms shown as insets in Fig. 4 and Fig. 5. The characterization of the spent catalysts with pre-reduced nanoparticles indicated that all the samples experienced a slight increase in the average nanoparticle size after six consecutive reaction runs, which, according to the results of the catalytic activity shown in Fig. 3, significantly affected the performance

Table 2
Average nanoparticle size and dispersion determined from TEM analysis.

Catalyst	d_{TEM} (nm)	D (%)
Pd/AS	3.8 ± 2.1	23.7
Pd/AS used	4.4 ± 1.9	20.5
Pd/N-AS	3.2 ± 0.9	28.1
Pd/N-AS used	3.6 ± 1.0	25.0
PdAg/AS	5.0 ± 2.0	18.0
PdAg/AS used	6.6 ± 2.6	13.6
PdAg/N-AS	2.8 ± 0.5	32.1
PdAg/N-AS used	4.0 ± 0.7	22.5
Pd/AS (n.r.)	–	–
Pd/AS (n.r.) used	4.5 ± 1.5	20.0
Pd/N-AS (n.r.)	–	–
Pd/N-AS (n.r.) used	2.9 ± 0.9	31.0
PdAg/AS (n.r.)	–	–
PdAg/AS (n.r.) used	6.9 ± 2.7	13.0
PdAg/N-AS (n.r.)	–	–
PdAg/N-AS (n.r.) used	6.4 ± 3.2	14.1

of most catalysts. Among those analyzed samples, fresh PdAg/N-AS catalyst had the smaller average nanoparticle size together with a very narrow particle size distribution (i.e., 2.8 ± 0.5 nm), which is in good agreement with the superior performance observed for that sample. The spent PdAg/N-AS still maintains a narrow particle size distribution although with a small increase in particle size (4.0 ± 0.7 nm). However, the spent PdAg/AS catalyst showed the largest average nanoparticle size (i.e., 6.6 ± 2.6 nm), which may be also related to their poorer stability compared to the other samples assessed. Nevertheless, extracting a direct relationship between the nanoparticle size and both activity and stability of the studied system is not a straightforward issue, which is due to the diversity of aspects that may affect the performance of the samples aside from the size of the nanoparticles (i.e., the composition of the nanoparticles, presence of nitrogen, and preparation method).

Concerning the catalysts that were *in-situ* reduced (denoted as "n.r."), the micrographs recorded for the spent catalysts (results shown in Figure S1) evidenced that the catalysts contain nanoparticles that were formed under reaction conditions. The average nanoparticle size determined for these catalysts indicated that, after six reaction cycles, the *in-situ* formed monometallic Pd nanoparticles are small and well-dispersed (average size of 4.5 ± 1.5 and 2.9 ± 0.9 nm, for Pd/AS (n.r) used and Pd/N-AS (n.r) used, respectively), and the effect of N-functional groups in serving as anchoring sites for the metal species was also seen. However, the bimetallic PdAg counterpart catalysts had larger and less dispersed particles (6.9 ± 2.7 and 6.4 ± 3.2 nm, for PdAg/AS (n.r.) used and PdAg/N-AS (n.r.) used, respectively), which is in good agreement with the poor activity shown by these samples (Fig. 3(c) and (d)).

As for the electronic properties of the Pd species, Fig. 6 and Figure S2 show the Pd 3d spectra of all the analyzed fresh and spent catalysts. It is known that the typical Pd 3d XPS spectrum displays two peaks related to Pd $3d_{5/2}$ (at lower binding energies) and Pd $3d_{3/2}$ (at higher binding energies) electron transitions, each of which can be deconvoluted into different peaks that correspond to the presence of Pd species with different electronic properties [52]. As expected, the fresh non-reduced samples only showed the contribution of Pd^{2+} related to the presence of the precursor used in the synthesis ($Pd(OAc)_2$) (see Figure S2) [53]. The XPS spectrum of the spent catalysts with non-prereduced nanoparticles showed in Figure S2 confirmed the reduction of metal species under reaction conditions, which is evidenced by the presence of the contribution related to Pd^0 in the samples denoted as Pd/AS (n.r.) used, Pd/N-AS (n.r.) used, PdAg/AS (n.r.) used, and PdAg/N-AS (n.r.) used. These *in-situ* reduced samples still showed the contribution of Pd^{2+} in the XPS spectra and, it should be noticed that while the N-free catalysts (Pd/AS (n.r.) used and PdAg/AS (n.r.) used) showed the typical signal of Pd^0 and Pd^{2+}, in the N-containing samples (Pd/N-AS (n.r.) used and PdAg/N-AS (n.r.)) the peaks related to Pd^{2+} appeared at higher binding energy, indicating the presence Pd species with a more electron-deficient

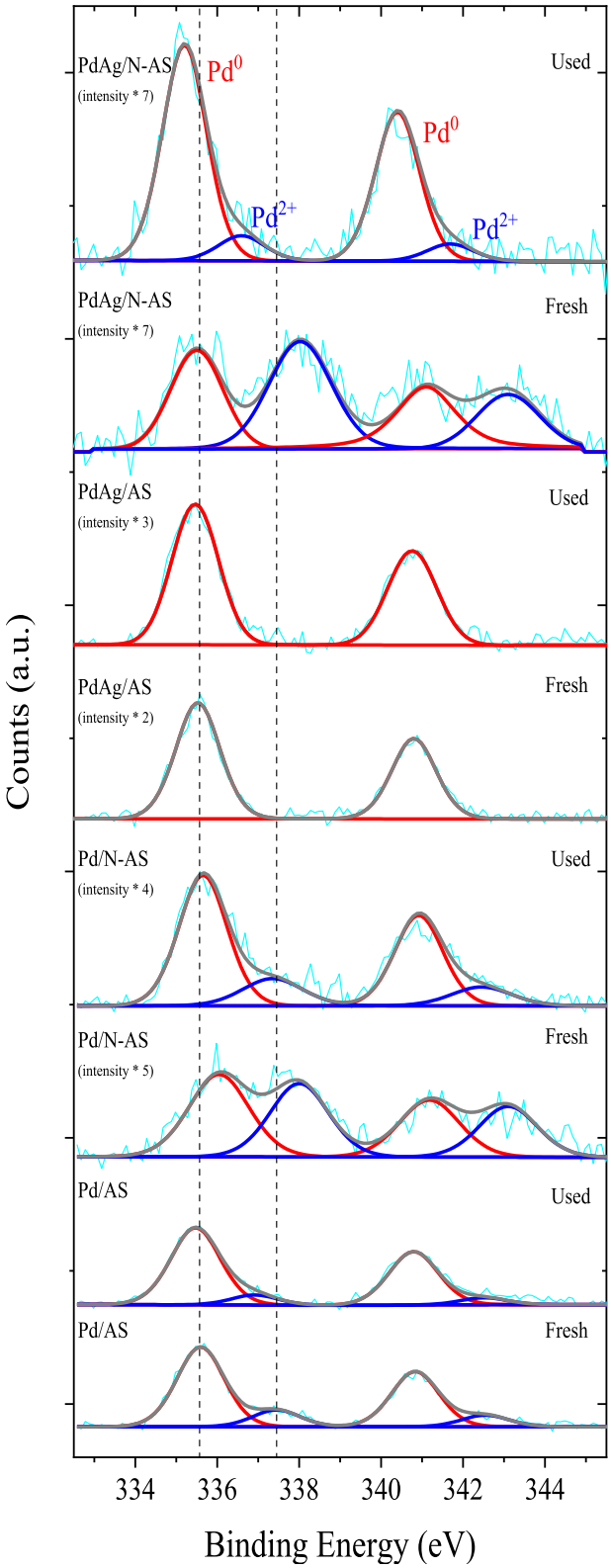

Fig. 6. Pd 3d XPS spectra of previously reduced fresh and used catalysts.

character. That may be related to the strong interaction between the Pd precursor used and the nitrogen functional groups as well as the role of nitrogen in stabilizing Pd^{2+} species [21]. Concerning the catalysts with pre-reduced nanoparticles (Pd/AS, Pd/N-AS, PdAg/AS, and PdAg/N-AS) displayed in Fig. 6, different tendencies were observed. In Pd/AS both

fresh and used, Pd^0 was the main species. Pd^{2+} was also detected on the surface of the samples and it had a very similar ratio in both fresh and used catalysts (17 and 11 %, respectively). In the case of the fresh N-containing counterpart, Pd/N-AS, the relative amount of Pd^{2+} is much higher than that in Pd/AS (46 and 17 %, respectively) and it is reduced considerably after reaction (21 % in used Pd/N-AS), but still higher than that of the N-free equivalent sample (11 % in Pd/AS used). Interestingly, PdAg/AS, both fresh and used, showed very symmetric peaks, indicating that only Pd^0 was present in the samples. That observation is in good agreement with previous studies in which the electronic enrichment of Pd surface atoms was identified upon alloying with Ag to form PdAg bimetallic nanoparticles [14,15,19]. However, the N-containing PdAg bimetallic catalysts showed the presence of Pd^{2+}, which again confirmed the strong Pd^{2+}-N interaction. The relative proportion of electron-deficient Pd species in PdAg/N-AS significantly decreased in the used catalyst (52 and 11 % in PdAg/N-AS and PdAg/N-AS used catalysts, respectively), but surface electron-deficient Pd species could still be detected. As for the effect of the incorporation of Ag in the nanoparticles, it favors the formation of electron-rich Pd species, which is particularly evident in sample PdAg/AS in which no Pd^{2+} was detected. It should be noticed that such an effect is somehow overshadowed in N-containing samples, since, as previously discussed, N-functional groups have the opposite effect, so elucidating the individual effect of N and Ag in the electronic properties of Pd species is not straightforward.

As previously mentioned, finding a direct relationship between each of the properties of the catalysts and the catalytic performance of the samples is very difficult considering the complexity of the studied system. However, the superior performance displayed by PdAg/N-AS may result from the sum of the features of this catalyst. On the one hand, that sample had well-dispersed and small particles with an average size of 2.8 ± 0.5 nm, which is much smaller compared to the N-free counterpart catalysts (5.0 ± 2.0 nm), thus pointing out the role of the nitrogen functional groups serving as anchoring points for the metal species. The presence of such nitrogen functionalities is also known to provide a basic character to the catalyst compared to the N-free samples, which is also beneficial to boost the dehydrogenation of FA and to increase the local concentration of FA molecules close to the active sites of the catalyst [28]. On the other hand, the electronic properties of the Pd species may also affect the final catalytic performance shown by the samples. In this sense, it has been reported that the presence of both Pd in the metallic state and Pd species with an electron-deficient character is needed to efficiently catalyze the dehydrogenation of FA [15,27,54]. It has been herein observed that the electronic properties of Pd species can be modulated by both incorporating a second element in the nanoparticles or by introducing a heteroatom in the carbon support. In this study, Ag and N have been selected as second element and heteroatom, respectively, to attain Pd-based catalysts supported on biomass-derived carbon supports. It has been demonstrated that, upon optimization of the experimental conditions used in the preparation of the catalysts, the strategy tackled is suitable to afford efficient catalysts with great stability under reaction conditions, which is one of the most desirable yet challenging characteristics pursued in the catalysts developed so far to boost the dehydrogenation of FA.

4. Conclusions

The present study reports on the development of Pd-based biomass-derived carbon-supported catalysts for the dehydrogenation of formic acid in the liquid phase. A total of 8 catalysts were prepared to explore the effect of (1) composition of the metal active phase as either monometallic Pd or PdAg bimetallic nanoparticles, (2) nitrogen incorporation in both monometallic and bimetallic PdAg catalysts, and (3) effect of the synthesis of the catalysts by using pre-reduced and *in-situ* reduced catalysts. The combination of the incorporation of Ag in the metal phase and the introduction of N-functional groups in the support, resulted, upon selection of a suitable synthetic protocol, in catalysts with promising activity and excellent stability under reaction conditions. Among the investigated samples, PdAg/N-AS showed the most promising results, with an initial TOF number of 1577 h^{-1}, which is higher than those of the Ag-free and N-free counterpart catalysts. The superior performance of PdAg/N-AS can be attributed to the small and well-dispersed nanoparticles present in that sample, as well as to the electronic properties of the Pd species which have resulted in excellent hydrogen formation rates with very good stability over six reaction cycles. The positive role of the nitrogen functional groups in attaining small nanoparticles is also demonstrated, which, together with their contribution to the basicity of the catalysts and hence favored interaction with formic acid molecules, resulted in crucial aspects to achieve promising catalysts for the studied application.

CRediT authorship contribution statement

Jessica Chaparro-Garnica: Conceptualization, Methodology, Investigation, Writing – original draft. **Miriam Navlani-García:** Conceptualization, Methodology, Investigation, Writing – original draft, Writing – review & editing, Supervision, Funding acquisition. **David Salinas-Torres:** Conceptualization, Methodology, Investigation, Writing – original draft, Writing – review & editing. **Ángel Berenguer-Murcia:** Conceptualization, Methodology, Writing – review & editing, Supervision. **Emilia Morallón:** Conceptualization, Methodology, Writing – review & editing, Supervision, Project administration, Funding acquisition. **Diego Cazorla-Amorós:** Conceptualization, Methodology, Writing – review & editing, Project administration, Funding acquisition.

Declaration of Competing Interest

The authors declare that they have no known competing financial interests or personal relationships that could have appeared to influence the work reported in this paper.

Acknowledgements

This work was financed by the MICINN, FEDER (RTI2018-095291-B-I00). JCG thanks for her predoctoral scholarship (GRISOLIA/2018/105) funded by the Generalitat Valenciana. MNG would like to thank the Plan GenT project from Generalitat Valencia (CDEIGENT/2018/027), and the Vicerrectorado de Investigación y Transferencia de Conocimiento de la Universidad de Alicante (GRE20-19-A) for the financial support.

References

[1] U.S. Environmental Protection Agency. https://www.epa.gov/ghgemissions/understanding-global-warming-potentials. Accessed 16 December 2021.
[2] Center for Climate and Energy Solutions. https://www.c2es.org/content/international-emissions. Accessed 19 December 2021.
[3] Garba MD, Usman M, Khan S, Shehzad F, Galadima A, Ehsan MF, et al. CO_2 towards Fuels: A Review of Catalytic Conversion of Carbon Dioxide to Hydrocarbons. J Environ Chem Eng 2021;9(2):104756. https://doi.org/10.1016/j.jece.2020.104756.
[4] U.S. Environmental Protection Agency. https://www.epa.gov/ghgemissions/overview-greenhouse-gases. Accessed 4 December 2021.
[5] Samanta S, Srivastava R. Catalytic Conversion of CO_2 to Chemicals and Fuels: The Collective Thermocatalytic/Photocatalytic/Electrocatalytic Approach with Graphitic Carbon Nitride. Mater Adv 2020;1(6):1506–45. https://doi.org/10.1039/D0MA00293C.

[6] Mazari SA, Hossain N, Basirun WJ, Mubarak NM, Abro R, Sabzoi N, et al. An Overview of Catalytic Conversion of CO_2 into Fuels and Chemicals Using Metal Organic Frameworks. Process Saf Environ Prot 2021;149:67–92. https://doi.org/10.1016/j.psep.2020.10.025.

[7] Fernández-Catalá J, Navlani-García M, Berenguer-Murcia Á, Cazorla-Amorós D. Exploring Cu_xO-Doped TiO_2 Modified with Carbon Nanotubes for CO_2 Photoreduction in a 2D-Flow Reactor. J CO_2 Util 2021;54:101796. https://doi.org/10.1016/j.jcou.2021.101796.

[8] Chen X, Liu Y, Wu J. Sustainable Production of Formic Acid from Biomass and Carbon Dioxide. Mol Catal 2020;483:110716. https://doi.org/10.1016/j.mcat.2019.110716.

[9] Enthaler S, Von Langermann J, Schmidt T. Carbon Dioxide and Formic Acid - The Couple for Environmental-Friendly Hydrogen Storage? Energy Environ Sci 2010;3(9):1207–17. https://doi.org/10.1039/b907569k.

[10] Gallas-Hulin A, Mielby J, Kegnæs S. Efficient Production of Hydrogen from Decomposition of Formic Acid over Zeolite Incorporated Gold Nanoparticles. ChemistrySelect 2016;1(13):3942–5. https://doi.org/10.1002/slct.201600831.

[11] Gao Y, Hu E, Yin G, Huang Z. Pd Nanoparticles Supported on CeO_2 Nanospheres as Efficient Catalysts for Dehydrogenation from Additive-Free Formic Acid at Low Temperature. Fuel 2021;302:121142. https://doi.org/10.1016/j.fuel.2021.121142.

[12] Ye W, Huang H, Zou W, Ge Y, Lu R, Zhang S. Controllable Synthesis of Supported PdAu Nanoclusters and Their Electronic Structure-Dependent Catalytic Activity in Selective Dehydrogenation of Formic Acid. ACS Appl Mater Interfaces 2021;13(29):34258–65. https://doi.org/10.1021/acsami.1c07740.

[13] Gu X, Lu ZH, Jiang HL, Akita T, Xu Q. Synergistic Catalysis of Metal-Organic Framework-Immobilized Au-Pd Nanoparticles in Dehydrogenation of Formic Acid for Chemical Hydrogen Storage. J Am Chem Soc 2011;133(31):11822–5. https://doi.org/10.1021/ja200122f.

[14] Wen M, Mori K, Futamura Y, Kuwahara Y, Navlani-García M, An T, et al. PdAg Nanoparticles within Core-Shell Structured Zeolitic Imidazolate Framework as a Dual Catalyst for Formic Acid-Based Hydrogen Storage/Production. Sci Rep 2019;9(1):15675. https://doi.org/10.1038/s41598-019-52133-5.

[15] Mori K, Dojo M, Yamashita H. Pd and Pd−Ag Nanoparticles within a Macroreticular Basic Resin: An Efficient Catalyst for Hydrogen Production from Formic Acid Decomposition. ACS Catal 2013;3(1):1114–9. https://doi.org/10.1021/cs400148n.

[16] Mori K, Tanaka H, Dojo M, Yoshizawa K, Yamashita H. Synergic Catalysis of PdCu Alloy Nanoparticles within a Macroreticular Basic Resin for Hydrogen Production from Formic Acid. Chem - A Eur J 2015;21:12085–92. https://doi.org/10.1002/chem.201501760.

[17] Mori K, Naka K, Masuda S, Miyawaki K, Yamashita H. Palladium Copper Chromium Ternary Nanoparticles Constructed In Situ within a Basic Resin: Enhanced Activity in the Dehydrogenation of Formic Acid. ChemCatChem 2017;9(18):3456–62. https://doi.org/10.1002/cctc.201700595.

[18] Navlani-García M, Mori K, Wen M, Kuwahara Y, Yamashita H. Size Effect of Carbon-Supported Pd Nanoparticles in the Hydrogen Production from Formic Acid. Bull Chem Soc Jpn 2015;1370(10):78–80. https://doi.org/10.1080/03758397.1955.10857269.

[19] Navlani-García M, Mori K, Nozaki A, Kuwahara Y, Yamashita H. Screening of Carbon-Supported PdAg Nanoparticles in the Hydrogen Production from Formic Acid. Ind Eng Chem Res 2016;55(28):7612–20. https://doi.org/10.1021/acs.iecr.6b01635.

[20] Ortega-Murcia A, Navlani-García M, Morallón E, Cazorla-Amorós D. MWCNT-Supported PVP-Capped Pd Nanoparticles as Efficient Catalysts for the Dehydrogenation of Formic Acid. Front Chem 2020;8:359. https://doi.org/10.3389/fchem.2020.00359.

[21] Navlani-García M, Salinas-Torres D, Vázquez-Álvarez FD, Cazorla-Amorós D. Formic Acid Dehydrogenation Attained by Pd Nanoparticles-Based Catalysts Supported on MWCNT-C_3N_4 Composites. Catal Today 2021. https://doi.org/10.1016/j.cattod.2021.07.019.

[22] Bulushev DA, Zacharska M, Shlyakhova EV, Chuvilin AL, Guo Y, Beloshapkin S, et al. Single Isolated Pd^{2+} Cations Supported on N-Doped Carbon as Active Sites for Hydrogen Production from Formic Acid Decomposition. ACS Catal 2016;6(2):681–91. https://doi.org/10.1021/acscatal.5b02381.

[23] Navlani-García M, Salinas-Torres D, Mori K, Léonard AF, Kuwahara Y, Job N, et al. Insights on Palladium Decorated Nitrogen-Doped Carbon Xerogels for the Hydrogen Production from Formic Acid. Catal Today 2019;324:90–6. https://doi.org/10.1016/j.cattod.2018.06.013.

[24] Nishchakova AD, Bulushev DA, Stonkus OA, Asanov IP, Ishchenko AV, Okotrub AV, et al. Effects of the Carbon Support Doping with Nitrogen for the Hydrogen Production from Formic Acid over Ni Catalysts. Energies 2019;12(21):4111. https://doi.org/10.3390/en12214111.

[25] Navlani-García M, Salinas-Torres D, Cazorla-Amorós D. Hydrogen Production from Formic Acid Attained by Bimetallic Heterogeneous PdAg Catalytic Systems. Energies 2019;12(21):4027. https://doi.org/10.3390/en12214027.

[26] Navlani-García M, Salinas-Torres D, Mori K, Kuwahara Y, Yamashita H. Enhanced Formic Acid Dehydrogenation by the Synergistic Alloying Effect of PdCo Catalysts Supported on Graphitic Carbon Nitride. Int J Hydrogen Energy 2018;44(53):28483–93. https://doi.org/10.1016/J.IJHYDENE.2018.11.057.

[27] Chaparro-Garnica J, Navlani-García M, Salinas-Torres D, Morallón E, Cazorla-Amorós D. Highly Stable N-Doped Carbon-Supported Pd-Based Catalysts Prepared from Biomass Waste for H_2 Production from Formic Acid. ACS Sustain Chem Eng 2020;8(39):15030–43. https://doi.org/10.1021/acssuschemeng.0c05906.

[28] Chaparro-Garnica J, Navlani-García M, Salinas-Torres D, Morallón E, Cazorla-Amorós D. H_2 Production from Formic Acid Using Highly Stable Carbon-Supported Pd-Based Catalysts Derived from Soft-Biomass Residues: Effect of Heat Treatment and Functionalization of the Carbon Support. Materials 2021;14(21):6506. https://doi.org/10.3390/ma14216506.

[29] Chaparro-Garnica J, Salinas-Torres D, Mostazo-López MJ, Morallón E, Cazorla-Amorós D. Biomass Waste Conversion into Low-Cost Carbon-Based Materials for Supercapacitors: A Sustainable Approach for the Energy Scenario. J Electroanal Chem 2021;880:114899. https://doi.org/10.1016/j.jelechem.2020.114899.

[30] Thommes M, Kaneko K, Neimark AV, Olivier JP, Rodriguez-Reinoso F, Rouquerol J, et al. Physisorption of Gases, with Special Reference to the Evaluation of Surface Area and Pore Size Distribution (IUPAC Technical Report). Pure Appl Chem 2015;87(9–10):1051–69. https://doi.org/10.1515/pac-2014-1117.

[31] Jagiello J, Olivier JP. 2D-NLDFT Adsorption Models for Carbon Slit-Shaped Pores with Surface Energetical Heterogeneity and Geometrical Corrugation. Carbon 2013;55(2):70–80. https://doi.org/10.1016/j.carbon.2012.12.011.

[32] Wu J, Wang K, Li Y, Yu P. Semihydrogenation of Phenylacetylene Catalyzed by Palladium Nanoparticles Supported on Organic Group Modified Silica. In Advanced Materials Research 2011;233–235:2109–12. https://doi.org/10.4028/www.scientific.net/AMR.233-235.2109.

[33] Bi QY, Lin JD, Liu YM, He HY, Huang FQ, Cao Y. Dehydrogenation of Formic Acid at Room Temperature: Boosting Palladium Nanoparticle Efficiency by Coupling with Pyridinic-Nitrogen-Doped Carbon. Angew Chemie - Int Ed 2016;55(39):11849–53. https://doi.org/10.1002/anie.201605961.

[34] Ping Y, Yan JM, Wang ZL, Wang HL, Jiang Q. $Ag_{0.1}$-$Pd_{0.9}$/rGO: An Efficient Catalyst for Hydrogen Generation from Formic Acid/Sodium Formate. J Mater Chem A 2013;1(39):12188–91. https://doi.org/10.1039/c3ta12724a.

[35] Deng Q-F, Xin J-J, Ma S-K, Cui F-J, Zhao Z-L, Jia L-H. Hydrogen Production from the Decomposition of Formic Acid over Carbon Nitride-Supported AgPd Alloy Nanoparticles. Energy Technol 2018;6(12):2374–9. https://doi.org/10.1002/ente.201800402.

[36] Bulut A, Yurderi M, Karatas Y, Say Z, Kivrak H, Kaya M, et al. MnO_x-Promoted PdAg Alloy Nanoparticles for the Additive-Free Dehydrogenation of Formic Acid at Room Temperature. ACS Catal 2015;5(10):6099–110. https://doi.org/10.1021/acscatal.5b01121.

[37] Gao S-T, Liu W, Feng C, Shang N-Z, Wang C. A Ag-Pd Alloy Supported on an Amine-Functionalized UiO-66 as an Efficient Synergetic Catalyst for the Dehydrogenation of Formic Acid at Room Temperature. Catal Sci Technol 2016;6(3):869–74. https://doi.org/10.1039/c5cy01190f.

[38] Feng C, Hao Y, Zhang L, Shang N, Gao S, Wang Z, et al. AgPd Nanoparticles Supported on Zeolitic Imidazolate Framework Derived N-Doped Porous Carbon as an Efficient Catalyst for Formic Acid Dehydrogenation. RSC Adv 2015;5(50):39878–83. https://doi.org/10.1039/C5RA04157K.

[39] Zhao X, Dai P, Xu D, Tao X, Liu X, Ge Q. Ultrafine PdAg Alloy Nanoparticles Anchored on NH_2-Functionalized 2D/2D TiO_2 Nanosheet/rGO Composite as Efficient and Reusable Catalyst for Hydrogen Release from Additive-Free Formic Acid at Room Temperature. J Energy Chem 2021;59:455–64. https://doi.org/10.1016/j.jechem.2020.11.018.

[40] Akbayrak S. Decomposition of Formic Acid Using Tungsten(VI) Oxide Supported AgPd Nanoparticles. J Colloid Interface Sci 2019;538:682–8. https://doi.org/10.1016/j.jcis.2018.12.074.

[41] Yang L, Hua X, Su J, Luo W, Chen S, Cheng G. Highly Efficient Hydrogen Generation from Formic Acid-Sodium Formate over Monodisperse AgPd Nanoparticles at Room Temperature. Appl Catal B Environ 2015;168–169:423–8. https://doi.org/10.1016/j.apcatb.2015.01.003.

[42] Wan C, Zhou L, Xu S, Jin B, Ge X, Qian X, et al. Defect Engineered Mesoporous Graphitic Carbon Nitride Modified with AgPd Nanoparticles for Enhanced Photocatalytic Hydrogen Evolution from Formic Acid. Chem Eng J 2022;429:132388. https://doi.org/10.1016/j.cej.2021.132388.

[43] Nabid MR, Bide Y, Etemadi B. Ag@Pd Nanoparticles Immobilized on a Nitrogen-Doped Graphene Carbon Nanotube Aerogel as a Superb Catalyst for the Dehydrogenation of Formic Acid. New J Chem 2017;41(19):10773–9. https://doi.org/10.1039/C7NJ01108C.

[44] Zhang Z, Luo Y, Liu S, Yao Q, Qing S, Lu Z-H. A PdAg-CeO_2 Nanocomposite Anchored on Mesoporous Carbon: A Highly Efficient Catalyst for Hydrogen Production from Formic Acid at Room Temperature. J Mater Chem A 2019;7(37):21438–46. https://doi.org/10.1039/c9ta06987a.

[45] Zhang X, Shang N, Zhou X, Feng C, Gao S, Wu Q, et al. AgPd-MnO_x supported on Carbon Nanospheres: An Efficient Catalyst for Dehydrogenation of Formic Acid. New J Chem 2017;41(9):3443–9. https://doi.org/10.1039/c6nj03873e.

[46] Dai H, Xia B, Wen L, Du C, Su J, Luo W, et al. Synergistic Catalysis of AgPd@ZIF-8 on Dehydrogenation of Formic Acid. Appl Catal B Environ 2015;165:57–62. https://doi.org/10.1016/J.APCATB.2014.09.065.

[47] Wan C, Yao F, Li X, Hu K, Ye M, Xu L, et al. Bimetallic AgPd Nanoparticles Immobilized on Amine-Functionalized SBA-15 as Efficient Catalysts for Hydrogen

Generation from Formic Acid. ChemistrySelect 2016;1(21):6907–13. https://doi.org/10.1002/slct.201601518.
[48] Choi B-S, Song J, Song M, Goo BS, Lee YW, Kim Y, et al. Core-Shell Engineering of Pd–Ag Bimetallic Catalysts for Efficient Hydrogen Production from Formic Acid Decomposition. ACS Catal 2019;9(2):819–26. https://doi.org/10.1021/acscatal.8b04414.
[49] Feng C, Wang Y, Gao S, Shang N, Wang C. Hydrogen Generation at Ambient Conditions: AgPd Bimetal Supported on Metal-Organic Framework Derived Porous Carbon as an Efficient Synergistic Catalyst. Catal Commun 2016;78:17–21. https://doi.org/10.1016/j.catcom.2016.01.034.
[50] Xu L, Jin B, Zhang J, Cheng D-G, Chen F, An Y, et al. Efficient Hydrogen Generation from Formic Acid Using AgPd Nanoparticles Immobilized on Carbon Nitride-Functionalized SBA-15. RSC Adv 2016;6(52):46908–14. https://doi.org/10.1039/c6ra06071d.
[51] Hattori M, Einaga H, Daio T, Tsuji M. Efficient Hydrogen Production from Formic Acid Using TiO_2-Supported AgPd@Pd Nanocatalysts. J Mater Chem A 2015;3:4453–61. https://doi.org/10.1039/C4TA06988A.
[52] Navlani-García M, Miguel-García I, Berenguer-Murcia Á, Lozano-Castelló D, Cazorla-Amorós D, Yamashita H. Pd/Zeolite-Based Catalysts for the Preferential CO Oxidation Reaction: Ion-Exchange, Si/Al and Structure Effect. Catal Sci Technol 2016;6(8):2623–32. https://doi.org/10.1039/c5cy02044a.
[53] Wang C-A, Nie K, Song G-D, Li Y-W, Han Y-F. Phenanthroline-Based Microporous Organic Polymer as a Platform for an Immobilized Palladium Catalyst for Organic Transformations. RSC Adv 2019;9(15):8239–45. https://doi.org/10.1039/C9RA00460B.
[54] Lv Q, Meng Q, Liu W, Sun N, Jiang K, Ma L, et al. Pd–PdO Interface as Active Site for HCOOH Selective Dehydrogenation at Ambient Condition. J Phys Chem C 2018;122(4):2081–8. https://doi.org/10.1021/acs.jpcc.7b08105.